High Li^+-Ion Storage Capacity and Double-Electrochromic Behavior of Sol−Gel-Derived Iron Oxide Thin Films with Sulfate Residues

Zhongchun Wang,*[,†,‡] Xingfang Hu,[†] Per-Olov Käll,[‡] and Ulf Helmersson[‡]

Shanghai Institute of Ceramics, Chinese Academy of Sciences, Shanghai 200050, People's Republic of China, and Department of Physics, Linköping University, SE-581 83 Linköping, Sweden

Received August 16, 2000. Revised Manuscript Received March 21, 2001

$FeSO_4 \cdot 7H_2O$ was precipitated with ammonia solution in the presence of H_2O_2 as an oxidant. The precipitate was washed slightly with deionized water and then peptized with acetic acid (ca. 60 mol %) to attain a homogeneous sol. Iron oxide films were fabricated by spin-coating the sol onto ITO-coated glass substrates and annealing at 350 °C or above. Structural and compositional analyses were done by TG-DTA, FTIR, XRD, TEM, and XPS. The results showed that sulfate residues were adsorbed on the surface of the Fe_2O_3 nanoparticles constituting the films by monodentate coordination with Fe(III) surface sites when heat treatment was carried out at ≤450 °C, while a conversion to bidentate occurred at 500 °C. As shown by the cyclic voltammograms results, the films annealed at 350 °C exhibited Li^+-ion storage capacity as high as ca. 0.50 $mC \cdot cm^{-2}$ per nanometer of the film thickness and showed double-electrochromic behavior depending on the extent of intercalation during the electrochemical lithium insertion/extraction processes. It is proposed that the adsorbed sulfate residues lead to the enhanced electroactivity of the iron oxide films by retarding crystallization and dehydration of the films. The high charge capacity and nearly optical passiveness of the iron oxide films suggest their promising applications as counter-electrodes in electrochromic devices.

Introduction

Iron oxides have three representative crystal structures, that is, α-Fe_2O_3 (corundum), γ-Fe_2O_3 (spinel), and Fe_3O_4 (spinel). Iron(III) oxide thin films are widely used for their interesting properties, for example, as catalysts in dehydrogenation reactions, magnetic devices, temperature and humidity sensors, optical filters, potential use in nonlinear optics, and so forth.[1,2] Iron oxide could also be considered as a promising electrochromic (EC) material with regard to its many valence states, which could be easily changed by either heat treatment or potential cycling in electrochemical cells. However, few studies have been done on the electrochromic properties of iron oxide films in its pure[3−6] or mixed oxide forms.[7−10]

Fe_2O_3 shows mixed cathodic/anodic electrochromism, which upon lithium intercalation, colors in the visible spectral region ($450 < \lambda < 800$ nm) and bleaches in the UV spectral region ($300 < \lambda < 450$ nm).[9] Its electrochromic mechanism is not well understood yet, but might be tentatively explained by band gap widening upon electrochemical reduction, analogous to that of V_2O_5.[11] It was shown that well-ordered α-Fe_2O_3, irrespective of the precursors used in their preparation, did not produce electrochromic properties of the α-Fe_2O_3 films,[5] and good electrochromic films have been either amorphous or γ-Fe_2O_3.[5] The sol−gel-derived films were typically fired at low temperatures (ca. 300 °C). Therefore, long-range disorder of iron oxide films seems to be a prerequisite for their electrochromism.

The importance of sulfate inclusion in α-Fe_2O_3-based ceramic gas sensors was found in the early 1980s. α-Fe_2O_3 is generally gas-insensitive because of its high chemical stability. However, α-Fe_2O_3 ceramics without any noble metal catalyst, prepared by precipitating an iron salt containing sulfate ions (SO_4^{2-}), were found to exhibit remarkable gas sensitivity.[12,13] This sensitivity is considered to be due to the fine crystallites and low crystallinity of the α-Fe_2O_3 induced by the existence of residual sulfate ions. Thus, the sulfate ions are considered to play a significant role in both producing the gas sensitivity and controlling the microstructure.

* To whom correspondence should be addressed. Present address: Departmento de Engenharia de Materiais Instituto Superior Tecnico, Av. Rovisco Pais, 1049-001 Lisboa, Portugal. Tel.: +351-21-8418109. Fax: +351-21-3145843. E-mail: spencer@ist.utl.pt.

† Chinese Academy of Sciences.

‡ Linköping University.

(1) Armelao, L.; Bertoncello, R.; Crociani, L.; Depaoli, G.; Granozzi, G.; Tondello, E.; Bettinelli, M. *J. Mater. Chem.* **1995**, *5*, 79.

(2) Armelao, L.; Granozzi, G.; Tondello, E.; Colombo, P.; Principi, G.; Lottici, P. P.; Antonioli, G. *J. Non Cryst. Solids* **1995**, *192/193*, 435.

(3) Zotti, G.; Schiavon, G.; Zecchin, S.; Casellato, U. *J. Electrochem. Soc.* **1998**, *145*, 385.

(4) Maruyama, T.; Kanagawa, T. *J. Electrochem. Soc.* **1996**, *143*, 1675.

(5) Orel, B.; Macek, M.; Svegl, F. *Thin Solid Films* **1994**, *246*, 131.

(6) Ozer, N.; Tepehan, F. *Sol. Energy Mater. Sol. Cells* **1999**, *56*, 141.

(7) Orel, B.; Macek, M.; Lavrencic-Stangar, U.; Pihlar, B. *J. Electrochem. Soc.* **1998**, *145*, 1607.

10.1021/cm000657j CCC: $20.00
Published on Web 05/19/2001

Sulfate treated α-Fe_2O_3 has been identified as a solid superacid, which effectively catalyze many commercially important reactions such as isomerization of lower paraffins at mild ambient conditions.[14] Surca et al.[15] prepared Ni-oxide films by the sol−gel route starting from sulfate salt and suggested that the retaining foreign ions (SO_4^{2-}, CO_3^{2-}, OH^-) are essential for the persistent electrochromism and stability of the films. Sulfation of goethite precursors and calcination at low temperature was proposed as a template-free route to the synthesis of mesoporous hematite.[16]

The hydrolysis process of metal ions in solutions has been reviewed in the literature.[17] The first step in the hydrolysis of Fe(III) ions in aqueous solutions is the formation of soluble iron polymers, which are converted into gels composed of polycations in a fractal arrangement. The hydrolysis continues with the precipitation of amorphous iron oxohydroxides that later transform into hematite (α-Fe_2O_3) or goethite (α-FeOOH). It has often been reported that the type of counterions in the precursor metal salt largely affects the hydrolysis of metal ions, which explains the difference in textures, magnetic, and other properties of the nanoparticles prepared from different metal salts. In the solution process, when the counterions restrain the transformation of amorphous ferrihydrite into a crystalline phase, the most stable phase, hematite, is formed. This effect increases in the following order: nitrate < chloride < sulfate.[18] It is also known that sulfate ions have a large affinity for iron oxide crystal surfaces that favors a rounded shape.[19,20]

In our previous works,[21] we prepared iron oxide nanoparticles by using $FeSO_4 \cdot 7H_2O$ as raw materials. Fe^{2+} ions were precipitated with ammonia as $Fe(OH)_2$, which is easily oxidized by air to form a greenish gray intermediate substance. The addition of H_2O_2 expedited the oxidation of $Fe(OH)_2$ and led to the instantaneous formation of large quantities of crystal nuclei under the weakly basic reaction medium. Because of their large amount, growth of these crystal nuclei was inhibited during the synthesis process, and therefore α-Fe_2O_3 particles with a diameter of ca. 10 nm and a specific surface area of 68.4 m^2/g were successfully prepared after firing at 400 °C for 2 h.

In the present work, we used the same method to prepare iron oxide nanoparticles, but the obtained precipitate was only slightly washed to include some SO_4^{2-} groups. Sols were made by peptizing the nanoparticles with acetic acid, and iron oxide films were fabricated by the spin-coating technique. The effects of sulfate inclusion on the structural and electrochromic properties of iron oxide films were extensively investigated.

Experimental Section

Sol Preparation and Thin Film Fabrication. The procedures to prepare iron oxide nanoparticles were detailed in our previous works.[21] $FeSO_4 \cdot 7H_2O$ was dissolved in deionized water to prepare 0.5 $mol \cdot L^{-1}$ $FeSO_4$ solution. Ammonium hydroxide solution (7 wt %) and H_2O_2 solution (6 wt %) were simultaneously added to the $FeSO_4$ solution with two microburets under stirring until pH $\sim$ 7 was reached. The $FeSO_4$ solution was kept at 70 °C with a water bath. The relative dripping rates of ammonium hydroxide and hydrogen peroxide were adjusted so that the greenish gray precipitate formed by the addition of ammonium hydroxide solution was just oxidized into a brownish yellow substance by the addition of H_2O_2 solution. The precipitate was filtered after aging for 2 h and then washed with deionized water only once.

Glacial acetic acid (ca. 60 mol %) was slowly added to the washed precipitate to attain peptization. A dark brown sol was obtained after stirring for 2 h. The viscous sol was used for making films by spin-coating onto indium−tin−oxide (ITO) conductive glass substrates (11 Ω/sq.). The films were fired in air in an oven at different temperatures for 1 h. The films studied in this work were made by only one spin, typical thickness being 100−150 nm depending on the firing temperatures.

Measurements. Thermal properties of the xerogel were investigated by TG-DTA analysis carried out on TA Instruments (TGA 2050, DSC 2910) at a heating rate of 10 °C/min in air. FTIR spectra of the xerogel powders after heat treatment in air at different temperatures for 2 h were recorded on a Perkin-Elmer spectrometer (Spectrum 1000) with N_2 purging using the conventional KBr pellet technique. The film thickness was measured by a Talystep profilometer. The structure of the films or the xerogel powders was investigated on a Philips PW 1820 powder diffractometer with Cu Kα radiation.

The iron oxide film was scraped from the substrate. The detritus was ground, dispersed in absolute alcohol, and scooped up with a copper grid to prepare samples for TEM analysis, which was carried out on a transmission electron microscope (TEM) JEOL 100CX with an accelerating voltage of 100 kV.

The chemical states and compositions of the films were analyzed by X-ray photoelectron spectroscopy (XPS) using a VG Microlab 310F system. XPS was carried out using a nonmonochromated Mg Kα (1253.6 eV) X-ray source, a hemispherical electron energy analyzer, and a takeoff angle of 90°. All the regional XPS spectra were calibrated with the binding energy of the adventitious C 1s peak (285 eV) or Au $4f^{7/2}$ (83.8 eV) for the lithiated films.

Cyclic voltammetry (CV) was carried out on iron oxide films immersed in an electrolyte of 1 $mol \cdot L^{-1}$ $LiClO_4$ in propylene carbonate (PC). A standard three-electrode arrangement was adopted with Pt as the counter-electrode and saturated calomel electrode (SCE) as the reference electrode. Constant and sweep potentials were provided by a potentiostat and a function generator, respectively. Optical properties of thin films were measured by a grating spectrophotometer. All data were collected under a dried atmosphere in a glove box, with a data acquisition system interfaced to a personal computer.

Results

Thermal Analysis of Iron Oxide Gel. TG and DTA curves of the iron oxide precursor xerogel are shown in

(8) Bencic, S.; Orel, B.; Surca, A.; Stangar, U. L. *Sol. Energy* **2000**, *68*, 499.
(9) Macek, M.; Orel, B.; Meden, T. *J. Sol−Gel Sci. Technol.* **1997**, *8*, 771.
(10) Surca, A.; Orel, B.; Krasovec, U. O.; Stangar, U. L.; Drazic, G. *J. Electrochem. Soc.* **2000**, *147*, 2358.
(11) Talledo, A.; Anderson, A. M.; Granqvist, C. G. *J. Mater. Res.* **1990**, *5*, 1253.
(12) Nakatani, Y.; Matsuoka, M. *Jpn. J. Appl. Phys.* **1982**, *21*, L758.
(13) Nakatani, Y.; Sakai, M.; Matsuoka, M. *Jpn. J. Appl. Phys.* **1983**, *22*, 912.
(14) Yamaguchi, T. *Appl. Catal.* **1990**, *61*, 1.
(15) Surca, A.; Orel, B.; Pihlar, B.; Bukovec, P. *J. Electroanal. Chem.* **1996**, *408*, 83.
(16) Baker, A. S. J.; Brown, A. S. C.; Edwards, M. A.; Hargreaves, J. S. J.; Kiely, C. J.; Meagher, A.; Pankhurst, Q. A. *J. Mater. Chem.* **2000**, *10*, 761.
(17) Matijevic, E. *Annu. Rev. Mater. Sci.* **1985**, *14*, 483. Flynn, C. M., Jr. *Chem. Rev.* **1984**, *84*, 31.
(18) Parida, K. M.; Das, J. *J. Mater. Sci.* **1996**, *31*, 2199.
(19) Park, G. S.; Shindo, D.; Waseda, Y.; Sugimoto, T. *J. Colloid Interface Sci.* **1996**, *177*, 198.
(20) Sugimoto, T.; Wang, Y. S. *J. Colloid Interface Sci.* **1998**, *207*, 137.
(21) Wang, Z.; Liu, E.; Chen, N.; Huang, J. *Chin. J. Struct. Chem.* **1996**, *15*, 450 (in Chinese). Wang, Z.; Liu, E.; Chen, N.; Huang, J. *Chin. J. Appl. Chem.* **1997**, *14*, 80 (in Chinese).

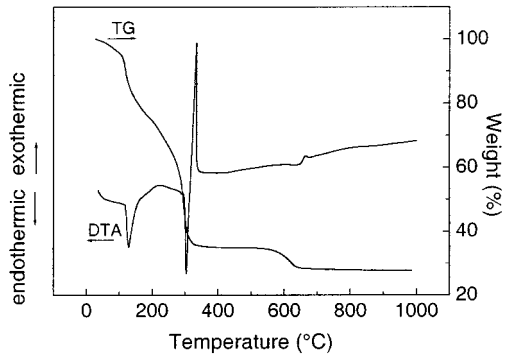

Figure 1. TG-DTA curves of iron oxide gel.

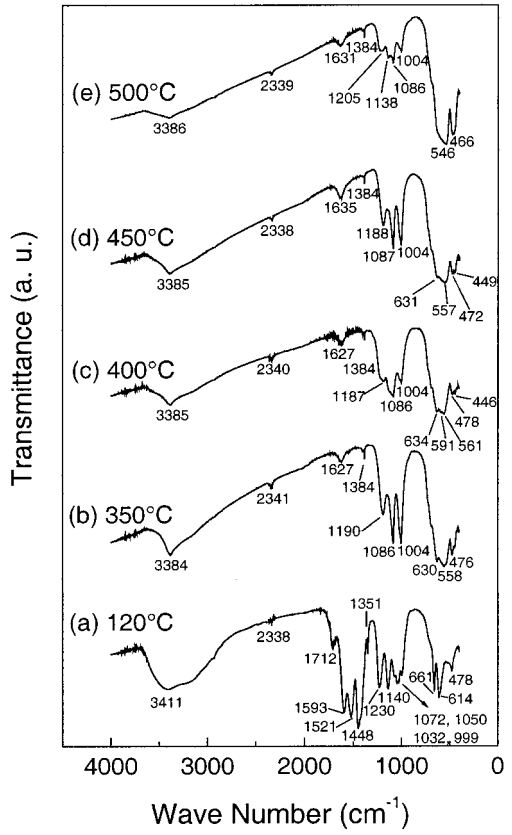

Figure 2. FTIR spectra of iron oxide xerogel powders dried or fired at different temperatures for 2 h.

Figure 1. On the DTA curve, an endothermic peak appears at 129 °C due to the loss of water and acetic acid. The two adjacent peaks at 304 and 335 °C could be ascribed to desorption and combustion of the acetate groups coordinated to Fe, respectively. One turn occurs at 664 °C on the DTA curve, accompanied by a weight loss of 7% on the TG curve. Considering the FTIR study described below, we tend to attribute this turn to desorption of sulfate residues, accompanied by complete dehydration.

On the basis of the thermal analysis results, we chose to anneal the film samples at temperatures between 350 and 550 °C, which resulted in the removal of organic residues while the sulfate residues remained in the films after the heat treatment.

FTIR Study. Figure 2 illustrates FTIR spectra of iron oxide xerogel powders dried or fired at different temperatures for 2 h. As shown in Figure 2a, the dried powder shows a broad absorption band at 3411 cm^{-1}, which can be assigned to the asymmetric and symmetric stretching modes of adsorbed water.[22] The broadness of this band also illustrates that a high amount of water is retained in the dried powder. The OH bending modes of water normally expected at 1640 cm^{-1} are hindered by the absorption at 1712 cm^{-1} ascribed to C═O mode from free acetic acid.

The bands at 1593 and 1448 cm^{-1} are due to the asymmetric and symmetric modes respectively of the monodentate acetate groups from the acetic acid used to peptize the precipitate.[5] The appearance of a band at 1521 cm^{-1} probably indicates that some of the monodentately bonded acetate groups have also transformed into chelating bidentate groups upon drying.[5]

Distinct absorption bands at 3385 cm^{-1} are observed in Figures 2b−e. Compared to the broad band observed in Figure 2a, this band is considerably sharper and its intensity decreases with increasing firing temperature. It can be ascribed to the stretching modes of H-bonded −OH groups in the xerogel powder, with the corresponding bending modes appearing at ∼1630 cm^{-1}. The presence of α-FeOOH was not confirmed due to the absence of characteristic bands at 896 and 797 cm^{-1}.[23] However, these bands were observed in the spectrum of the precipitate dried at 120 °C (data not shown here). Pejova et al.[24] have reported that complete dehydration took place and pure α-Fe_2O_3 was obtained by heat-treating precipitated FeOOH at 350−400 °C. In other words, the presence of sulfate groups in our samples seems to hold the hydroxyl groups in place until relatively higher temperatures are reached, although we have not ruled out the possibility that moisture might have been adsorbed by the xerogel powders during the brief exposures to the open air while making the KBr pellets for the FTIR measurements.

In Figures 2b−e, distinct bands from adsorbed CO_2 appear at ∼2340 cm^{-1} (ν_3), which cannot be explained simply by insufficient N_2 purging. Considering the highly active surface of the α-Fe_2O_3 powder, it is quite possible that CO_2 molecules were adsorbed during pyrolysis of the xerogel.

Free sulfate groups with T_d symmetry show a single band at 1104 cm^{-1}. In Figure 2, the single peak of a free sulfate group is split into at least three distinct peaks, indicating that the symmetry of the adsorbed sulfate is lowered due to coordination with surface Fe(III) sites.

Hug[25] has compared IR spectra of adsorbed sulfates to compounds with known coordination to distinguish various structures that sulfate can form with surface Fe(III) sites and found that a clear distinction between monodentate and bidentate coordination can be made based on the number of observed peaks. Monodentate coordination (C_{3v} symmetry) leads to three peaks and bidentate (C_{2v} symmetry) to four (plus an additional peak at ca. 1200 cm^{-1}). Eggleston et al.[26] also reported in their work on sulfate adsorption on hematite that the

(22) Bellamy, L. J. *The Infrared Spectra of Complex Molecules*; John Wiley & Sons Inc.: New York, 1954; Chapter 6, p 85.
(23) Jasinski, R.; Iob, A. *J. Electrochem. Soc.* **1988**, *135*, 551.
(24) Pejova, B.; Najdoski, M.; Grozdanov, I.; Isahi, A. *J. Mater. Sci.: Mater. Electron.* **2000**, *11*, 405.
(25) Hug, S. J. *J. Colloid Interface Sci.* **1997**, *188*, 415.
(26) Eggleston, C. M.; Hug, S.; Stumm, W.; Sulzberger, B.; Afonso, M. D. S. *Geochim. Cosmochim. Acta* **1998**, *62*, 585.

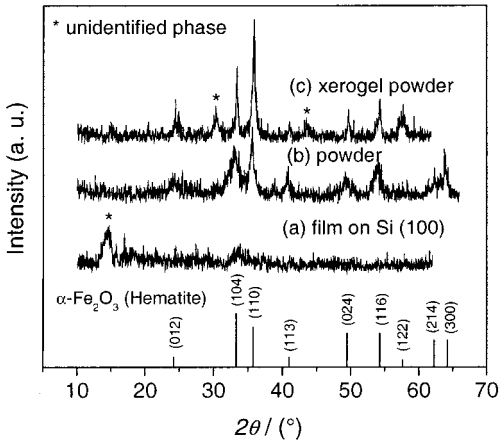

Figure 3. X-ray diffractograms of iron oxide samples fired at 400 °C for 1 h: (a) film deposited on Si(100); (b) dried powder from coprecipitation; (c) xerogel powder. Stick diagram of hematite is also shown for comparison.

appearance of a peak at or above 1200 cm^{-1} might reflect the formation of adsorbed bisulfate or sulfate−H_3O^+ structures.

In Figures 2b−d, for the samples annealed between 350 and 450 °C, three peaks are observed at 1004, 1086, and 1190 cm^{-1}, respectively, in agreement with monodentate coordination. However, more peaks in the $\nu_{S=O}$ region are observed for the 120 °C dried or 500 °C fired xerogel powders. In Figure 2a, two intense peaks appear at 1230 and 1140 cm^{-1} and four weaker ones at 1072, 1050, 1032, and 999 cm^{-1}, respectively. We believe these peaks originate from a mixture of monodentately coordinated sulfate and bisulfate ions, considering the appreciable amount of water that exists in the 120 °C dried xerogel powder. On the other hand, in Figure 2e, the four peaks observed at 1205, 1138, 1086, and 1004 cm^{-1} indicate that a change from monodentate to bidentate occurred after firing at 500 °C. The last assignment is also in agreement with the facts that sulfate-promoted α-Fe_2O_3 catalysts are typically calcined at 500 °C to activate the surface superacid sites and the coordination of sulfate groups to Fe has been assigned as chelating bidentates.[27,28]

In Figures 2b−e, broad absorption bands from α-Fe_2O_3 are observed at ∼550 and ∼470 cm^{-1}, which can be assigned to ν_1 and ν_3 modes, respectively.[29] The two bands were also observed by Koyande et al.[28] in the FTIR spectrum of the SO_4^{2-}/α-Fe_2O_3 catalyst after heat treatment at 500 °C. In the samples fired at temperatures lower than 500 °C, additional features are superimposed on the two bands, but specific assignments will not be attempted here.

XRD Study. Figure 3 shows the XRD-2θ scans of iron oxide samples after heat treatments in air at 400 °C for 1 h. The samples are (a) film deposited on a Si(100) wafer (ca. 100 nm in thickness), (b) iron oxide powder before peptizing with acetic acid, and (c) xerogel powder. The XRD powder patterns in Figures 3b and 3c can be indexed as α-Fe_2O_3 (hematite). The two peaks at 30.2° and 43.5° in Figure 3c might be ascribed to γ-Fe_2O_3, which is known to be more readily formed under a reducing atmosphere.[30] As seen in Figure 3b or 3c, the relative intensity of reflections from the (104) and (110) planes is reversed with regard to the standard; this preferential orientation was also observed by Baker et al.[16] and was ascribed to the sulfation effect. Besides, the peaks in Figure 3c are somewhat sharper and less shifted toward lower 2θ values as compared to those in Figure 3b. The exothermic thermo-decomposition of the adsorbed acetic acid might have promoted the crystal growth of iron oxide and also the formation of a reducing ambient.

The film sample did not exhibit well-defined peaks, as seen in Figure 3a. One diffuse peak appears at 2θ corresponding to the (104) peak of the α-Fe_2O_3 phase, and another broad peak, not identified yet, appears at a very low angle (14.5°).

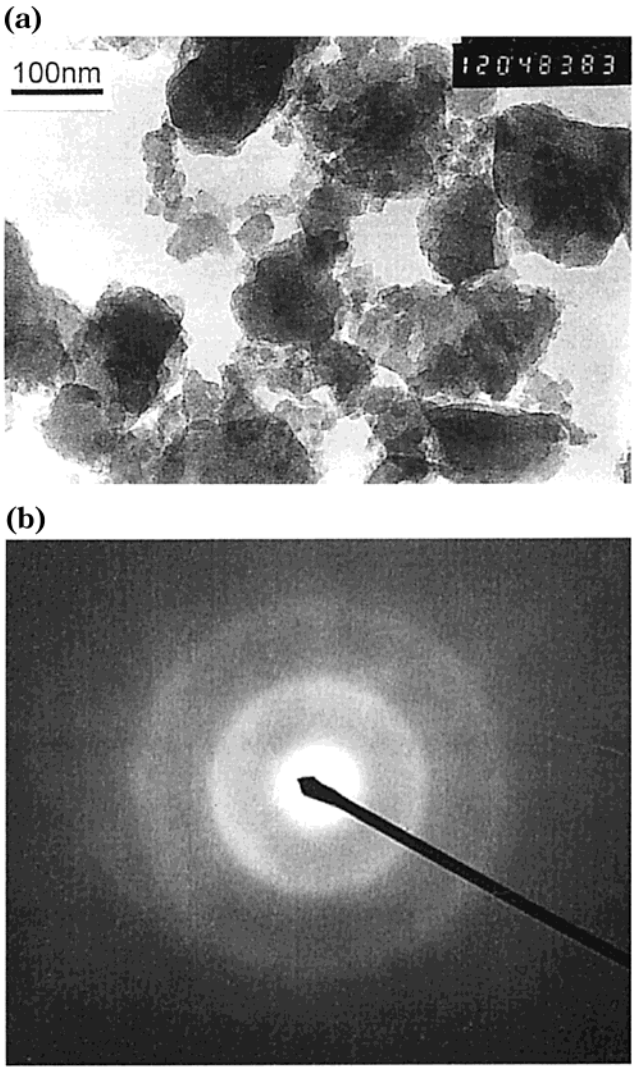

Figure 4. TEM image (a) and selected-area electron diffraction pattern (b) of the 350 °C fired iron oxide film.

TEM Study. Figure 4a shows a bright field image of detritus scraped from a 350 °C heated iron oxide film. It can be seen that the film was composed of agglomerated nanoparticles, the average size of which is esti-

(27) Yamaguchi, T.; Jin, T.; Ishida, T.; Tanabe, K. *Mater. Chem. Phys.* **1987**, *17*, 3.
(28) Koyande, S. N.; Jaiswal, R. G.; Jayaram, R. V. *Ind. Eng. Chem. Res.* **1998**, *37*, 908.
(29) Lawson, K. E.; Corporation, S.; Base, S.; Albuquerque, N. M. *Infrared Absorption of Inorganic Materials*; Reinhold Publishing Corp.: New York, 1961; p 62.
(30) Uekawa, N.; Kaneko, K. *J. Mater. Res.* **1999**, *14*, 2002.

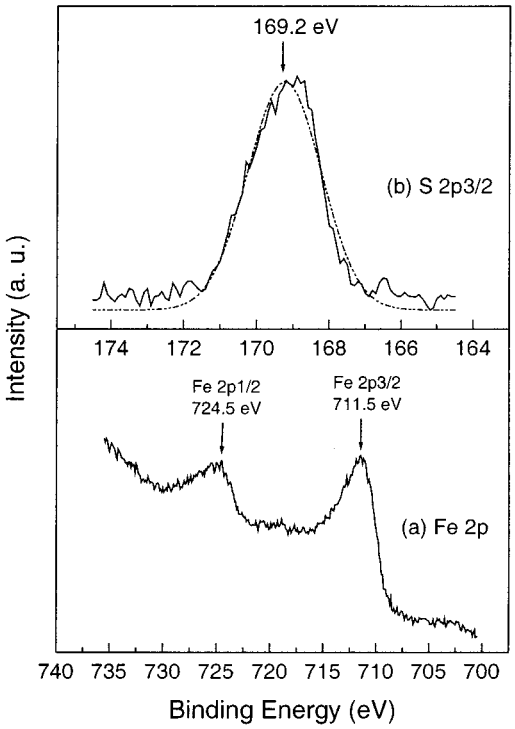

Figure 5. Fe 2p (a) and S $2p^{3/2}$ (b) XPS spectra of the 350 °C fired iron oxide film. In (a), the background is not subtracted. In (b), the dotted line is the Gaussian fit of the raw data.

mated to be ca. 10 nm. We did not observe the nanoporous structures as reported in ref 16, though more standard sample preparation techniques and HRTEM are needed to further examine this subject. The selected area electron diffraction pattern is shown in Figure 4b. Only faint diffuse rings are seen in the pattern, indicating that the film is essentially amorphous, in agreement with the XRD results.

XPS Analysis of Iron Oxide Films. The compositions and chemical states of the 350 °C heated iron oxide films were investigated with XPS. The spin−orbit doublet, Fe $2p^{3/2}$ and Fe $2p^{1/2}$, are located at 711.5 and 724.5 eV respectively, with a separation of 13.0 eV (Figure 5a), indicating the formation of Fe_2O_3 films.[31,32] Signals from S 2p photoelectrons were clearly observed. In Figure 5b, data from S $2p^{3/2}$ was fitted by a Gaussian function centered at 169.2 eV, in agreement with the binding energies of S $2p^{3/2}$ in SO_4^{2-}.[33,34]

Figure 6 represents the O 1s XPS spectrum, which has two components. The more intense peak at 532.0 eV can be ascribed to the oxygen from OH^- and adsorbed SO_4^{2-}. The other peak at 530.0 eV is due to iron oxide itself.[35]

From the above XPS analysis of the iron oxide films, we can conclude that the film surface is not coincident with $Fe_2(SO_4)_3$, but composed of Fe_2O_3 with SO_4^{2-}, which can be analogous to the sulfated Fe_2O_3 as a superacid catalyst.[14] In regard to the existence of OH^-

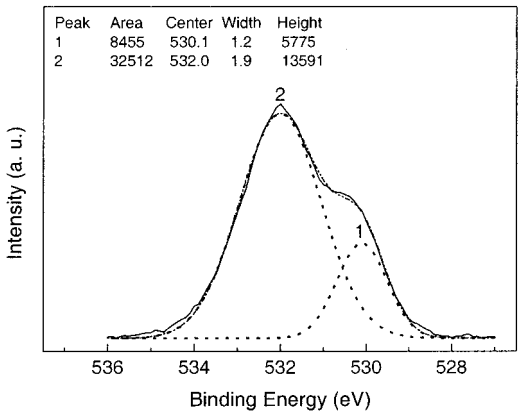

Figure 6. O 1s XPS spectrum of the 350 °C fired iron oxide film. Dotted lines are the fitted results.

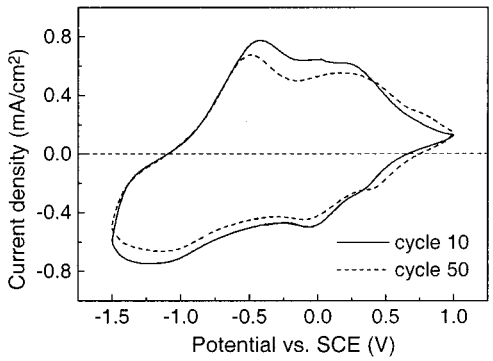

Figure 7. Cyclic voltammograms of the iron oxide film fired at 350 °C for 1 h with a thickness of 120 nm. Scan rate: 20 mV/s.

and SO_4^{2-} groups on the surface of the iron oxide particles constituting the films, the XPS results are also in agreement with the above FTIR results.

Electrochemical and Electrochromic Properties of Iron Oxide Films. Cyclic voltammetry experiments were performed in a potential range between −1.5 and +1 V (starting from +1 V) and at a scanning rate of 20 mV/s. Electrochromic properties of the 350 °C heated iron oxide films were investigated by in situ monochromatic transmittance measurements when Li^+/e^- were intercalated into the oxide matrix during the CV process, taking the electrochemical cell with electrolyte as a reference. Figure 7 shows data recorded during the 10th and the 50th cycles, while the data in Figures 8 and 9 are for the 10th cycle.

The shape of the voltammogram is typical for amorphous Fe_2O_3 films.[3] The broad cathodic peaks at ∼0 and ∼1.25 V might be correlated with the two redox processes to Fe_3O_4 and FeO, respectively. The corresponding anodic peaks occurred at ∼0.3 and ca. −0.4 V, respectively. Current response diminished slightly with cycling (Figure 7). By integration of the current response with time in Figure 7, the inserted and extracted charge densities (Q_c and Q_a) for the 10th cycle are calculated to be 56.5 and 48.2 mC/cm^2, respectively, with a reversibility (defined as the ratio of Q_a/Q_c) of 85.3%. For the 50th cycle, the reversibility increased to 86.5% (Q_c and Q_a are 51.0 and 44.1 mC/cm^2, respectively). The film thickness was 120 nm, so the charge capacity per film thickness (Q/d) can be as high as ∼0.50 mC·cm^{-2}·nm^{-1}, taking the inserted charge density for the 10th cycle. Assuming the density of our iron oxide films as 4 g/cm^3

(31) Wandelt, K. *Surf. Sci. Rep.* **1982**, *2*, 1.
(32) Briggs, D.; Seah, M. P. *Practical Surface Analysis*, 2nd ed.; Wiley: Chichester, 1990; Vol. 1.
(33) Toledano, D. S.; Dufresne, E. R.; Henrich, V. E. *J. Vac. Sci. Technol. A* **1998**, *16*, 1050.
(34) Descostes, M.; Mercier, F.; Thromat, N.; Beaucaire, C.; Gautier-Soyer, M. *Appl. Surf. Sci.* **2000**, *165*, 288.
(35) Bayon, R.; Maffiotte, C.; Herrero, J. *Thin Solid Films* **1999**, *353*, 100.

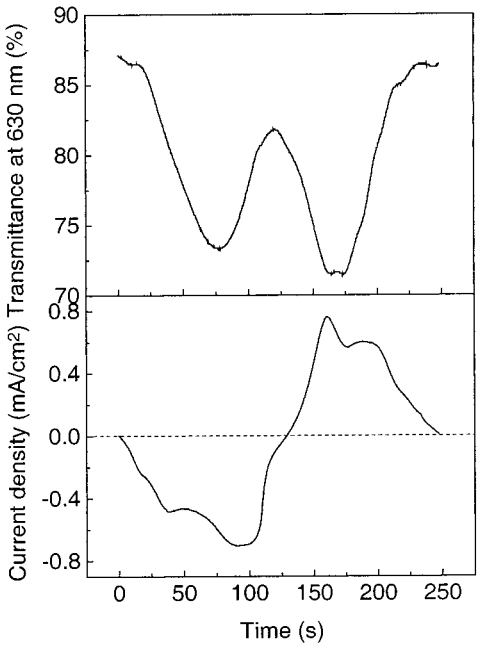

Figure 8. Current response and corresponding transmittance change as functions of time recorded in Figure 7 for the 10th cycle.

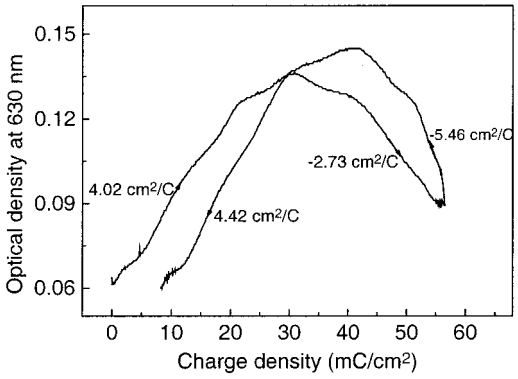

Figure 9. Change in optical density at 630 nm as a function of accumulated charge, calculated from the data in Figure 8.

(5.2 g/cm^3 for α-Fe_2O_3, hematite), we can approximate the lithium uptake of our iron oxide films as high as $Li_{1.9}Fe_2O_3$.

The Li^+-ion storage capacity of our Fe_2O_3 films is much higher than those reported for iron-oxide-based films in the literature.[5,9,36,37] In ref 5, a maximal Q/d value of ∼0.2 mC·cm^{-2}·nm^{-1} or a lithium uptake capability of 0.9−1.1 Li^+ per Fe_2O_3 was reported for a γ-Fe_2O_3 film heat-treated at 300 °C, as measured in 10^{-3} M KOH aqueous solution. In Macek et al.'s work,[9] sol−gel-derived Fe_2O_3−TiO_2 films were investigated electrochemically with the help of cyclic voltammetry and chronocoulometry performed in 10^{-2} M LiOH and were found to be able to uptake reversibly Li^+ ions with a charge capacity in the range 0.1−0.26 mC·cm^{-2}·nm^{-1}. However, this value was reduced to 0.06 mC·cm^{-2}·nm^{-1} when measured in 1 M $LiClO_4$/propylene carbonate electrolytes, as in our case. Our value is also higher than those of the best known ion storage films. Sputtered TiO_2−CeO_2 films showed a capacity of 18 mC/cm^2 with high reversibility.[38] Orel et al.[39] reported single-dipped SnO_2/Mo films (100−200-nm-thick) with a high ion storage capacity of 20−30 mC/cm^2 while Nb−Fe mixed oxide films[7] were up to 18 mC/cm^2. V_2O_5, which is ranked among the most promising ion storage films, typically possesses an ion storage capacity of up to 35 mC/cm^2.[36]

The cycling test was continued until the 250th cycle. No obvious change was observed except for a reduction of ∼5% in charge capacity.

Figure 8 contrasts the current response and the transmittance change at 630 nm during the 10th cycle. Upon lithium insertion in the cathodic half-cycle, the transmittance of the iron oxide film decreased at first and then increased; that is, it behaved cathodically in the former stage and anodically in the later stage. The opposite took place in the anodic half-cycle. In Figure 9, the optical densities (OD) are plotted against the charge density (Q), where Q was calculated by integrating the current response in Figure 8, and OD was calculated from the transmittance in Figure 8 according to OD = $-\log_{10} T$. The slopes of the linear sections represent coloration efficiencies at 630 nm, as marked in Figure 9. Negative values stand for anodic coloration. The absolute values of these CEs are less than 6 cm^2/C, which are comparable to 6.0−6.5 cm^2·C^{-1} for amorphous iron oxide films deposited by chemical vapor deposition,[4] but much lower than that of the sol−gel-derived iron oxide films, 28 cm^2/C,[6] as measured at 550 nm.

On the basis of the data in Figure 9, the coloration process observed at 630 nm during the 10th cycle can be written as follows:

$$Fe_2O_3 \xrightarrow{\text{cathodic}} Li_{1.0}Fe_3O_3 \xrightarrow{\text{anodic}} Li_{1.9}Fe_2O_3 \xrightarrow{\text{cathodic}} Li_{1.4}Fe_2O_3 \xrightarrow{\text{anodic}} Li_{0.2}Fe_2O_3 \quad (1)$$

where "cathodic/anodic" stands for "cathodic coloration/anodic coloration".

The coloration behavior observed here is analogous to that of V_2O_5 films observed in our former works.[40] Because of the double-electrochromic behavior (anodic and cathodic coloration) depending on the wavelength and the intercalation extent, the transmittance modulation range of the iron oxide films is limited. Figure 10 shows ex situ optical transmittance data for the Fe_2O_3 film in the as-deposited state, and in different intercalated states, which were measured by stopping the CV cycling at different points of one CV cycle. As can be seen in Figure 10, the film exhibited transmittance changes between the intercalated and de-intercalated states less than 10% for nearly the whole visible spectral region despite its high charge capacity. Photopic trans-

(36) Granqvist, C. G. *Handbook of Inorganic Electrochromic Materials*; Elsevier: Amsterdam, 1995. Aegerter, M. A. Sol−Gel Chromogenic Materials and Devices. In *Structure and Bonding* 85, 149; Springer-Verlag: Berlin, 1996.
(37) Campet, G.; Wen, S.; Han, S. D.; Shastry, M. C. R.; Portier, J.; Guizard, C.; Cot, L.; Xu, Y.; Salardenne, J. *Mater. Sci. Eng. B* **1993**, *18*, 201.
(38) Schlotter, P.; Baur, G.; Schmidt, R.; Weinberg, U. *Proc. SPIE-Int. Soc. Opt. Eng.* **1994**, 2255, 351. Camino, D.; Derro, D.; Salardenne, J.; Treuil, N. *Sol. Energy Mater. Sol. Cells* **1995**, *39*, 349.
(39) Krasovec, U. O.; Orel, B.; Hocevar, S.; Musevic, I. *J. Electrochem. Soc.* **1997**, *144*, 3398.
(40) Wang, Z.; Li, Z.; Chen, X.; Hu, X. *Acta Phys. Sin.-Ov. Ed.* **1999**, *8*, 57. Wang, Z.; Chen, J.; Hu, X. *Thin Solid Films* **2000**, *375*, 238.

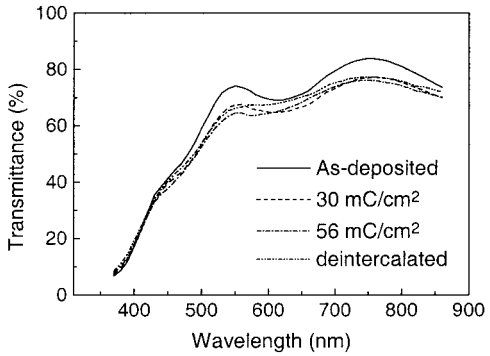

Figure 10. Transmittance spectra of the 350 °C fired iron oxide film at different states.

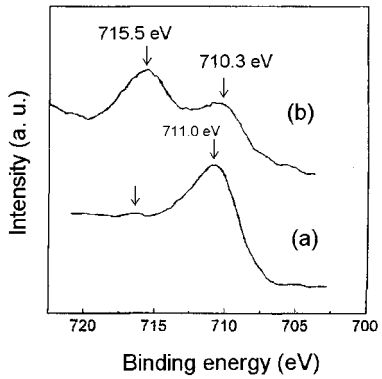

Figure 11. XPS Fe $2p^{3/2}$ spectra of the lithiated iron oxide film with different inserted charge densities: (a) 20 mC/cm^2 and (b) 40 mC/cm^2.

mittances (T_{vis}) for the four states are calculated to be 69.8, 64.0, 62.2, and 64.8%, respectively.

XPS Analysis of the Lithiated Iron Oxide Film. The process of lithium uptake of the 350 °C fired iron oxide film was further investigated by XPS. After lithium insertion to a charge density of 20 mC/cm^2, the Fe $2p^{3/2}$ XPS peak shifted to 711.0 eV with a small hump at 716.0 eV (Figure 11 a). With further lithiation to 40 mC/cm^2, the Fe $2p^{3/2}$ XPS peak shifted to 710.3 eV, and an intense broad peak appeared at 715.5 eV (Figure 11 b). According to Wandelt,[31] who has reviewed XPS characteristics of Fe $2p^{3/2}$ spectra of iron oxides, the peaks at 710.3 eV can be ascribed to Fe^{2+}, while the hump in Figure 11a and the peak at 715.5 eV in Figure 11b are the shake-up satellites from Fe^{2+}. From these results, that is, the shift of Fe $2p^{3/2}$ binding energy to lower values and the presence of an Fe^{2+} shake-up satellite with lithiation, we can conclude that Fe^{3+} in the iron oxide films is gradually reduced to Fe^{2+} with the double injection of lithium ions and electrons.

Discussion

Our FTIR and XPS results clearly show that both sulfate and water or hydroxyl groups are retained in the films fired at temperatures lower than 500 °C and that the adsorbed SO_4^{2-} ions are monodentately coordinated to surface Fe(III) sites. It is believed that the adsorption of sulfate groups leads to stronger Lewis acidity for Fe^{3+} ions as a result of induction effect,[41] and therefore Fe^{3+} ions more strongly attract electrons. For charge neutrality to be maintained, the Li^+ ions must follow the pace of electrons and are attracted to the Fe^{2+} sites. A higher rate of lithium insertion should thus be expected for iron oxide films with sulfate residues, as compared with pure Fe_2O_3 films.

The important role of an optimum amount of water to the electrochromic properties of WO_3 films is well-known, and Li^+ ion diffusion in the oxide becomes much easier when the film contains water.[42,43] Analogous to Pyun et al.'s study on hydrogen transport through H_2O-containing amorphous WO_3 films,[44] we can explain the accelerating role of water or hydroxyl groups incorporated in our Fe_2O_3 films to the Li^+ ion intercalation. On the surface of the nanoparticles, which are in direct contact with the aprotic electrolyte, Li^+ ions can easily move on via exchanging with the H^+ ions from the surface hydroxyl groups. A Li^+ ion may diffuse in the bulk of the nanoparticles by jumping to an adjacent lattice O^{2-} ion, or an OH group, or an H_2O molecule. Clearly, the bonding strength decreases following the order: $O^{2-}-Li^+ > OH^--Li^+ > H_2O-Li^+$, so it is reasonable to expect that Li^+ ions associated with an OH group or water are more mobile than those bound to O^{2-} ions.

We noticed that in ref 6 only a slight shift in binding energy for Fe $2p^{3/2}$ and Fe $2p^{1/2}$, 0.5 eV, was observed after the iron oxide film was electrochemically colored, and no satellite peak for Fe^{2+} was observed. We believe that the reasons behind the readiness in observing the presence of Fe^{2+} states after lithiation in our case lies in two aspects. One is the much deeper lithiation in our case (40 mC/cm^2 in Figure 11b). The other is related to the enhancing effect of sulfate residues on the reduction of Fe^{3+} to Fe^{2+}, as explained above.

The iron oxide films heated at 350 and 400 °C were tested with regard to their electrochromic properties. The 400 °C heated samples showed only slightly reduced electroactivity (data not shown here). Films heated at 500 °C or above tend to crack, probably because of loss of water and/or crystallite growth. In comparison with what was observed for pure Fe_2O_3 (ref 3) or MoO_3 films,[45] (that is, cyclability and electrochromic response decreased drastically upon crystallization induced by heat treatments at the same temperature range), it is obvious that the adsorbed sulfate residues have played an important role in retarding the dehydration and crystallization of the iron oxide films and keeping the charge capacity of the films until much higher temperatures.

Conclusions

In this work, nanoparticulate Fe_2O_3 thin films with sulfate residues were successfully fabricated. The sulfate inclusion has been found to inhibit dehydration and crystallization of the Fe_2O_3 films.

The Fe_2O_3 films showed charge capacity as high as $Li_{1.9}Fe_2O_3$, and double-electrochromic behavior, which makes the films nearly optically passive to lithium

(41) Kayo, A.; Yamaguchi, T.; Tanabe, K. *J. Catal.* **1983**, *83*, 99.
(42) Judeistein, P.; Livage, J. *Mater. Sci. Eng. B* **1989**, *3*, 129.
(43) Wang, Z.; Hu, X. *Electrochim. Acta* **2001**, *46*, 1951.
(44) Pyun, S. I.; Kim, D. J.; Bae, J. S. *J. Alloys Compd.* **1996**, *244*, 16.
(45) Guerfi, A.; Paynter, R. W.; Dao, L. H. *J. Electrochem. Soc.* **1995**, *142*, 3457.

insertion. These features fit with the requirements for counter-electrodes in electrochromic devices. However, it should be pointed out that an intrinsic drawback of the Fe_2O_3 films for counter-electrode applications, similar to V_2O_5 films,[46] would be the low transparency at the lower wavelengths in the visible spectral region ($<\sim$550 nm), which can only be alleviated by making a compromise between film thickness (corresponding to luminous transparency) and charge capacity. Besides, the cyclic stability of our Fe_2O_3 films needs to be further improved by optimizing the processing parameters, for example, the amount of sulfate residues and/or peptizing agents, the heat-treatment temperature and/or procedure.

(46) Zhang, J.-G.; Benson, D. K.; Tracy, C. E.; Deb, S. K.; Czanderna, A. W.; Crandall, R. S. *J. Electrochem. Soc.* **1994**, *141*, 2795.

Acknowledgment. This work was supported by the Climbing Programs of the State Commission of Science and Technology of China (Grant 07-01) and the National Natural Science Foundation of China (Grants 59782006 and 59932040).

CM000657J